

Fill and spill of giant lakes in the Eastern Valles Marineris region of Mars

Nicholas H. Warner^{1*}, Mariam Sowe², Sanjeev Gupta¹, Alexander Dumke² and Kate Goddard¹

¹ *Dept. Earth Science & Engineering, Imperial College London, South Kensington Campus, London, SW7 2AZ*

² *Institute of Geological Sciences, Planetary Sciences & Remote Sensing, Freie Universitaet Berlin, Malteserstrasse 74-100, D-12249 Berlin,*

** now at Jet Propulsion Laboratory, 4800 Oak Grove Dr., Pasadena, CA, 91109*

Methods

1. Image Mosaic Construction

A complete image mosaic (sinusoidal projection) was created to describe the geomorphology of the region encompassing Eos Chaos, Capri Chasma, and Aurorae Chaos. The mosaic utilized 150 Mars Reconnaissance Orbiter Context Camera (CTX) (Malin et al., 2007) image strips (Table DR1) at 6 m pixel⁻¹ resolution and several co-registered High Resolution Stereo Camera (HRSC) (Jaumann et al., 2007; Neukum et al., 2004) strips at 12.5-25 m pixel⁻¹ (depending on the ground resolution of the respective image) where CTX was lacking. The imagery was co-registered and georeferenced for mapping and crater chronology analysis in a Geographic Information System (ArcGIS 10.0).

2. HRSC Digital Terrain Model Construction Methods

The topographic analysis of the target study features, including basins, outflow channels and the interior layered deposits, was done using a high-resolution HRSC digital terrain model (DTM) (Fig. 1). The mosaic consists of 25 individual orbit strips and was overlaid by co-registered CTX and HRSC imagery to analyze relationships between observed landforms and topography. The DTM is firmly tied to Mars Global Surveyor Mars Orbiter Laser Altimeter data (MOLA) (Smith et al., 2001) with up to 100 m grid-spacing, with spheroid (and optional areoid) projection and equidistant projection (due to the near-equatorial position). Vertical accuracy corresponds to the resolution of the respective orthoimage; further information can be found in Gwinner et al. (2009).

3. Crater count methods for chronology determination

To determine the chronology of basin formation, we digitized and counted all craters larger than 2 km in diameter (D) on the floors of the Capri-Eos and Aurorae Chaotic terrains using the regional CTX and HRSC mosaic (sinusoidal projection) within ArcGIS 10.0. Craters were digitized using two points measured from the crater center to the rim. The minimum bound of this diameter range was chosen due to an observed roll-over in the data on cumulative frequency histograms in craterstats2 for the $D < 2$ km

population of basin floor craters. This rollover is likely due to multiple factors including the poor preservation of smaller diameter craters on the sloping surfaces of the chaos mounds, basin-floor fluvial erosion, partial burial by dust/interior layered material, or late stage wind modification. For craters in the diameter range of $D > 10^1$ km, a select few show evidence for disruption by formation of the chaotic terrains and therefore represent a pre-basin, highland crater population (Fig. DR3).

For the outflow channels and the upper mantled surface of Capri Mensa, we utilized only the high-resolution CTX images to count all craters with $D > 100$ m (Fig. DR8 for example craters on the outflow surfaces). Due to a rollover in the curves at $D < 200$ m, all fits on the outflow channels were applied to the $D > 200$ m diameter range. For Capri Mensa, a rollover in the cumulative frequency histogram is observed at $D < 300$ m. All secondary chains associated with the 48-km-diameter crater on Eos Mensa at 11.1° S, 322.9° E were avoided in the count. These chains contain km-sized impact structures that occur within range of the Daga Vallis, Columbia Valles, and Eos Chasma surfaces (Fig. DR9). Thus, it is possible that randomly-distributed km-sized secondaries from this crater that are outside of these chains were inadvertently included in the counts for each channel. This may account for the apparent “bulge” in the cumulative frequency histograms that systematically occurs for each channel at $D > 1$ km.

The countable areas for all flood and ILD surfaces exceed 10^3 km² and the total number of craters counted for each surface = 10^3 craters. To estimate absolute surface ages for all target features, we constructed cumulative crater-size-frequency histograms, providing fits to established isochrons using the chronology functions of Hartmann and Neukum (2001) and the production function of Ivanov (2001) in the craterstats2 software (Michael and Neukum, 2010). The chronologic boundaries of the Martian geologic epochs were chosen following Werner and Tanaka (2011). Table DR2 provides the cumulative crater frequency values for different diameter ranges.

- Gwinner, K., Scholten, F., Spiegel, M., Schmidt, R., Giese, B., Oberst, J., Heipke, C., Jaumann, R., and Neukum, G., 2009, Derivation and Validation of High-Resolution Digital Terrain Models from Mars Express HRSC Data: Photogrammetric Engineering and Remote Sensing, v. 75, no. 9, p. 1127-1142.
- Hartmann, W. K., and Neukum, G., 2001, Cratering Chronology and the Evolution of Mars: Space Science Review, v. 96, p. 165-194.
- Ivanov, B., 2001, Mars/Moon Cratering Rate Ratio Estimates: Space Science Reviews, v. 96, p. 87-104.
- Jaumann, R., Neukum, G., Behnke, T., Duxbury, T. C., Eichertopf, K., Flohrer, J., von Gasselt, S., Giese, B., Gwinner, K., Hauber, E., Hoffmann, H., Hoffmeister, A., Kohler, U., Matz, K. D., McCord, T. B., Mertens, V., Oberst, J., Pischel, R., Reiss, D., Ress, E., Roatsch, T., Saiger, P., Scholten, F., Schwarz, G., Stephan, K., Wahlisch, M., and Team, H. C.-I., 2007, The high-resolution stereo camera (HRSC) experiment on Mars Express: Instrument aspects and experiment conduct from interplanetary cruise through the nominal mission: Planetary and Space Science, v. 55, no. 7-8, p. 928-952.
- Malin, M. C., Bell, J. F., Cantor, B. A., Caplinger, M. A., Calvin, W. M., Clancy, R. T., Edgett, K. S., Edwards, L., Haberle, R. M., James, P. B., Lee, S. W., Ravine, M. A., Thomas, P. C., and Wolff, M. J., 2007, Context Camera Investigation on board the Mars Reconnaissance Orbiter: Journal of Geophysical Research-Planets, v. 112, no. E5.
- Michael, G. G., and Neukum, G., 2010, Planetary surface dating from crater size-frequency distribution measurements: Partial resurfacing events and statistical age uncertainty: Earth and Planetary Science Letters, v. 294, no. 3-4, p. 223-229.
- Neukum, G., Jaumann, R., and Team, H. C.-I., 2004, HRSC: The High Resolution Stereo Camera of Mars Express, ESA Special Publications SP-1240.
- Smith, D. E., Zuber, M. T., Frey, H. V., Garvin, J. B., Head, J. W., Muhleman, D. O., Pettengill, G. H., Phillips, R. J., Solomon, S. C., Zwally, H. J., Banerdt, W. B., Duxbury, T. C., Golombek, M. P., Lemoine, F. G., Neumann, G. A., Rowlands, D. D., Aharonson, O., Ford, P. G., Ivanov, A. B., Johnson, C. L., McGovern, P. J., Abshire,

J. B., Afzal, R. S., and Sun, X. L., 2001, Mars Orbiter Laser Altimeter: Experiment summary after the first year of global mapping of Mars: *Journal of Geophysical Research-Planets*, v. 106, no. E10, p. 23689-23722.
 Werner, S. C., and Tanaka, K. L., 2011, Redefinition of the crater-density and absolute-age boundaries for the chronostratigraphic system of Mars: *Icarus*, v. 215, no. 2, p. 603-607.

Data Repository Figures

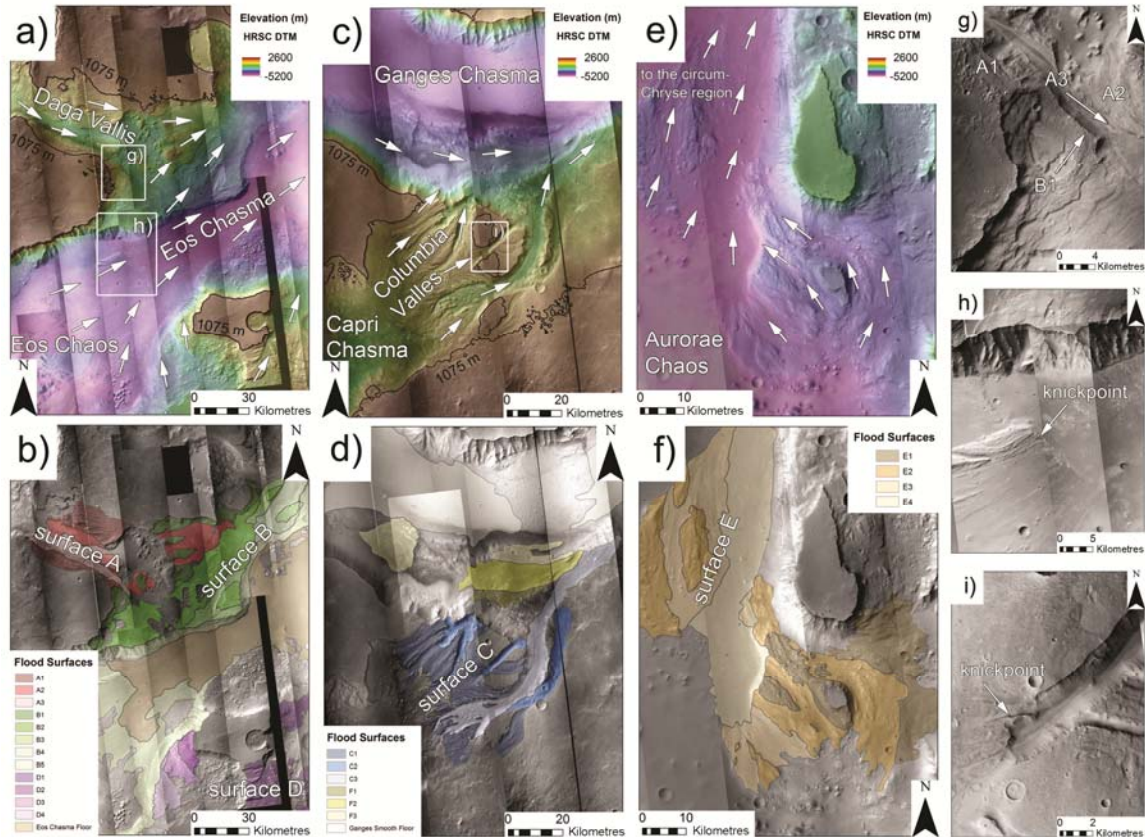


Figure DR1: HRSC topography and CTX imagery of all outflow channels associated with the Capri-Eos and Aurorae Chaos basins (a, c, e). Plates b, d, and f are geomorphic maps that display different flood erosion surfaces within each outflow channel. Each erosion surface represents evidence for progressive downcutting that occurred due to significant base level differences between the water source (i.e. lake surface) and the downstream basin. Plate g highlights the crosscutting relationships between channels that emerge from Capri Chasma and those that emerge from Eos Chaos. Plates h and i display preserved knickpoints on the floors of the outflow channels. These knickpoints suggest that flood erosion was accomplished through headward incision, likely a result of a topographic discontinuity/base level difference that existed between the water source and downstream basin.

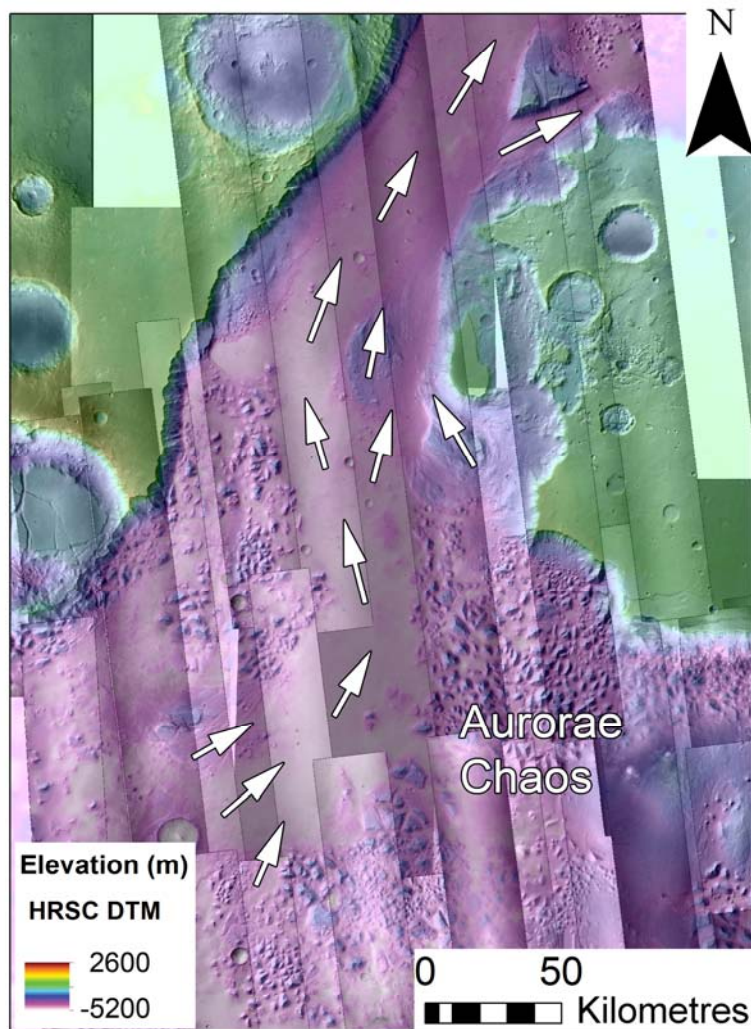


Figure DR2: CTX mosaic overlain by HRSC topography highlighting the north-central floor of Aurorae Chaos. Grooved terrains and smooth surfaces are interpreted here to represent evidence of water flow through this pre-existing basin. Water that passed through Aurorae Chaos was derived from the regions of Ganges Chasma and the Capri-Eos basin.

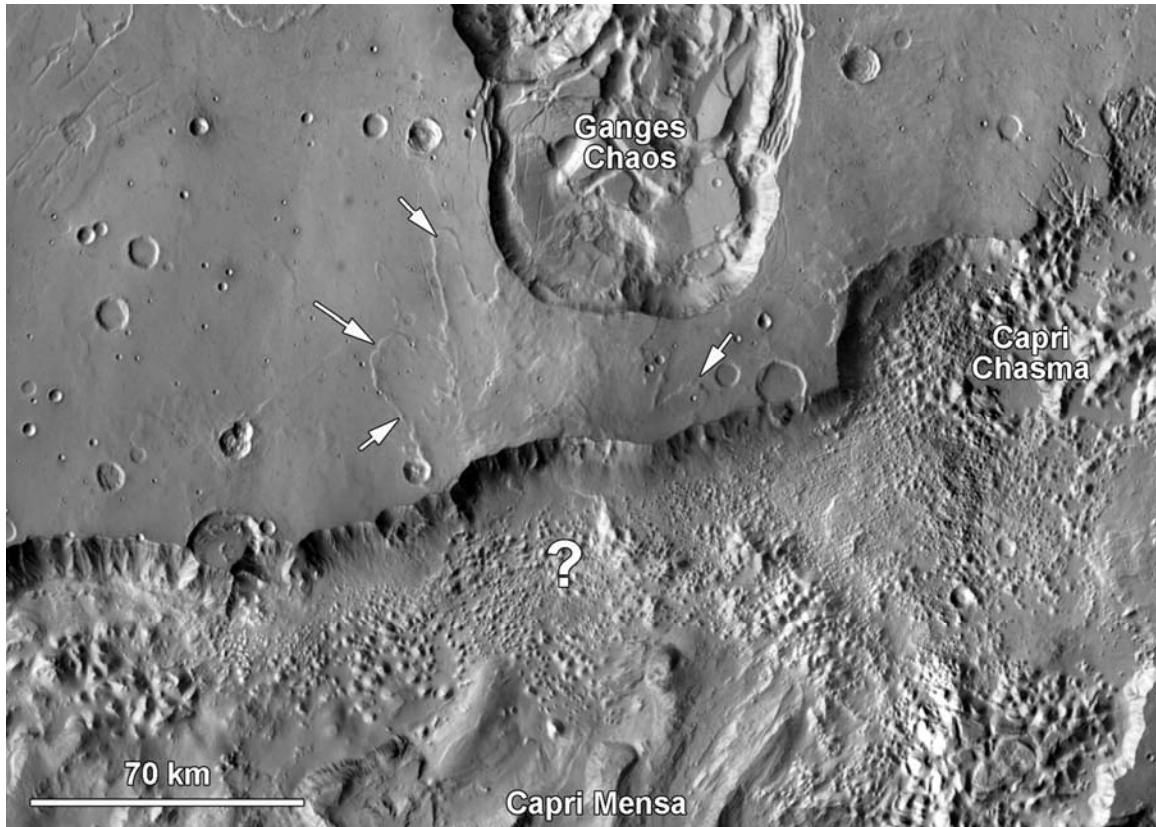


Figure DR3: THEMIS daytime mosaic of the northern margin of Capri Chasma. The mosaic displays a well-preserved lobate ejecta blanket that extends northward from the northern rim of Capri Chasma. The 10^1 km diameter source crater that formed the ejecta blanket has been completely destroyed by subsidence and disruption of the highland terrain. This indicates that the formation of Capri Chasma and its associated chaotic terrains (e.g. Eos Chaos) likely resulted in complete obliteration of most kilometer-sized impact craters that were initially present at this location on the highland surface. We suggest that $< 10^1$ km-sized craters on the floor of the basins therefore provide a lower-limit crater retention age of when the basins formed.

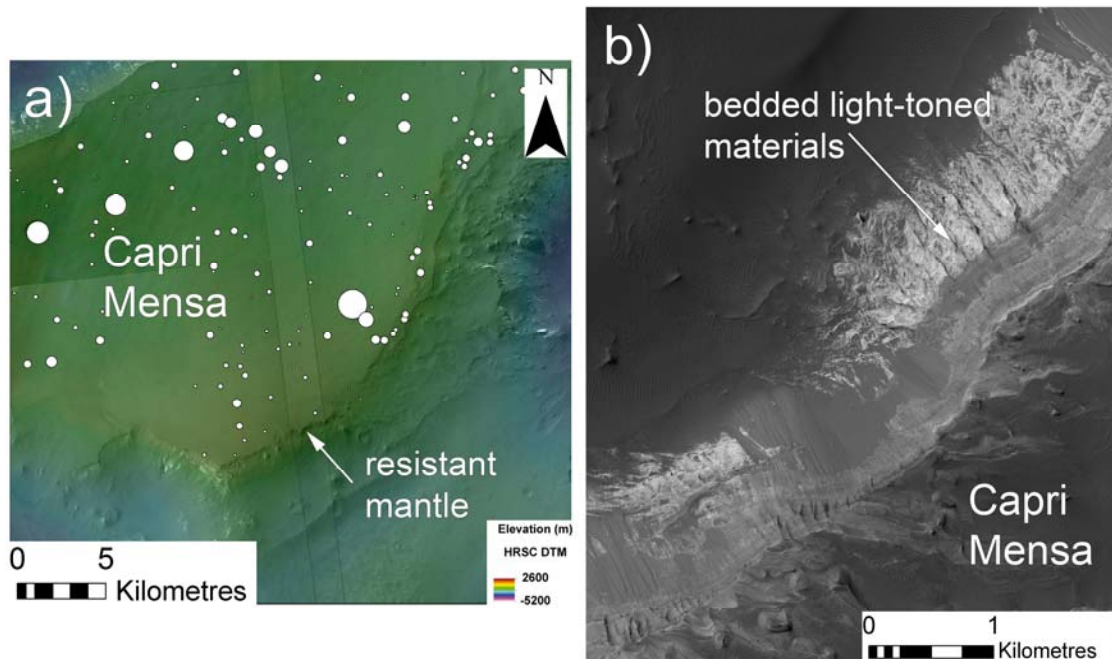


Figure DR4: Image mosaics and topography of the interior layered deposit in the Capri-Eos basin, Capri Mensa. a. CTX mosaic overlain by HRSC topography displaying the well-preserved mantle of the Capri Mensa mound. Impact crater statistics were acquired from this mantle to determine a surface crater retention age. The mantle was found to have a crater retention age of 3.1 Ga. b. High Resolution Imaging Science Experiment (HiRISE) image at 25 cm pixel^{-1} displaying an exposure of horizontally layered materials within the Capri Mensa mound. The layered units show no evidence for disruption by formation of the chaotic terrain that constitutes the Capri-Eos basin. This indicates that the ILD mound was deposited after the basin was formed.

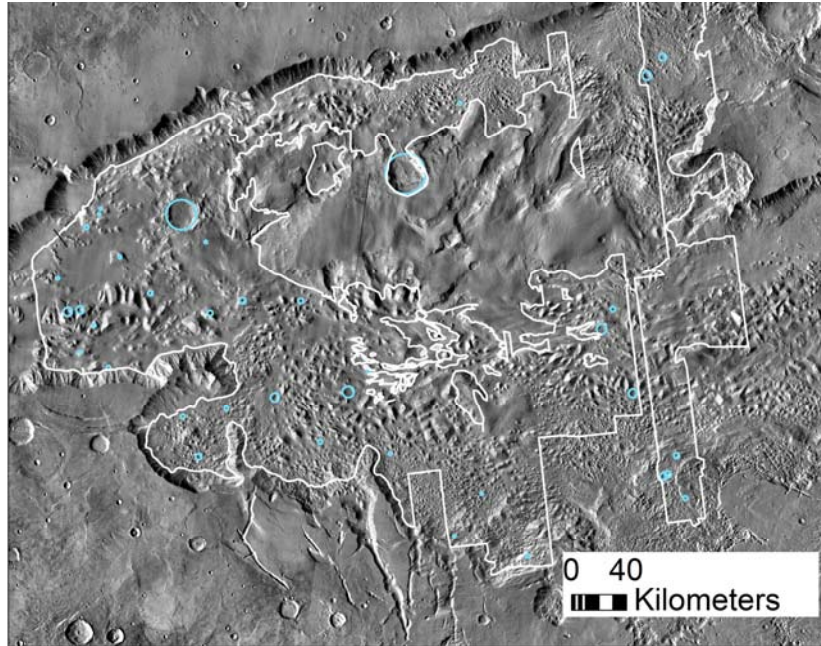


Figure DR5: THEMIS daytime IR mosaic of the Capri-Eos basin displaying the basin floor crater population ($D > 2$ km) and counted area (white).

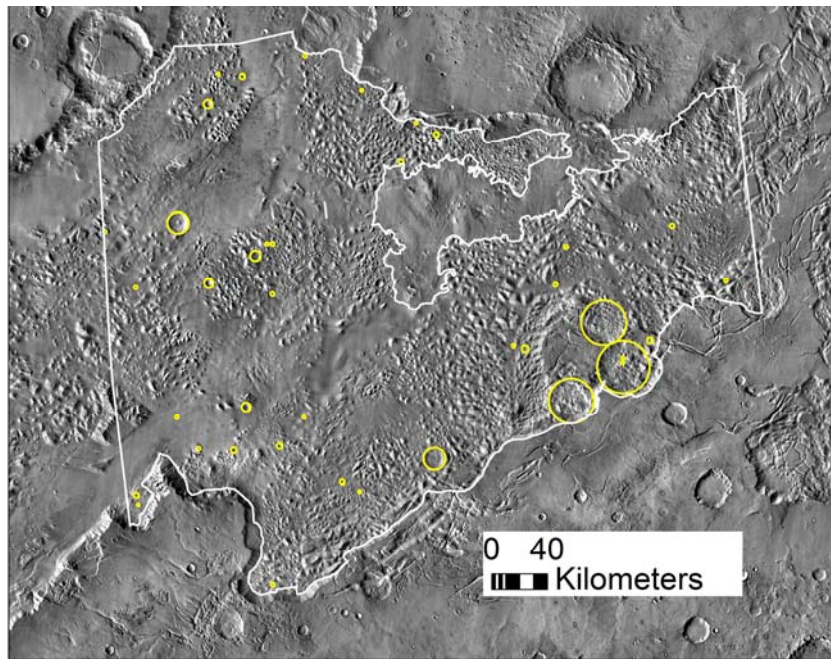


Figure DR6: THEMIS daytime IR mosaic of the Aurorae basin displaying the basin floor crater population ($D > 2$ km) and counted area (white).

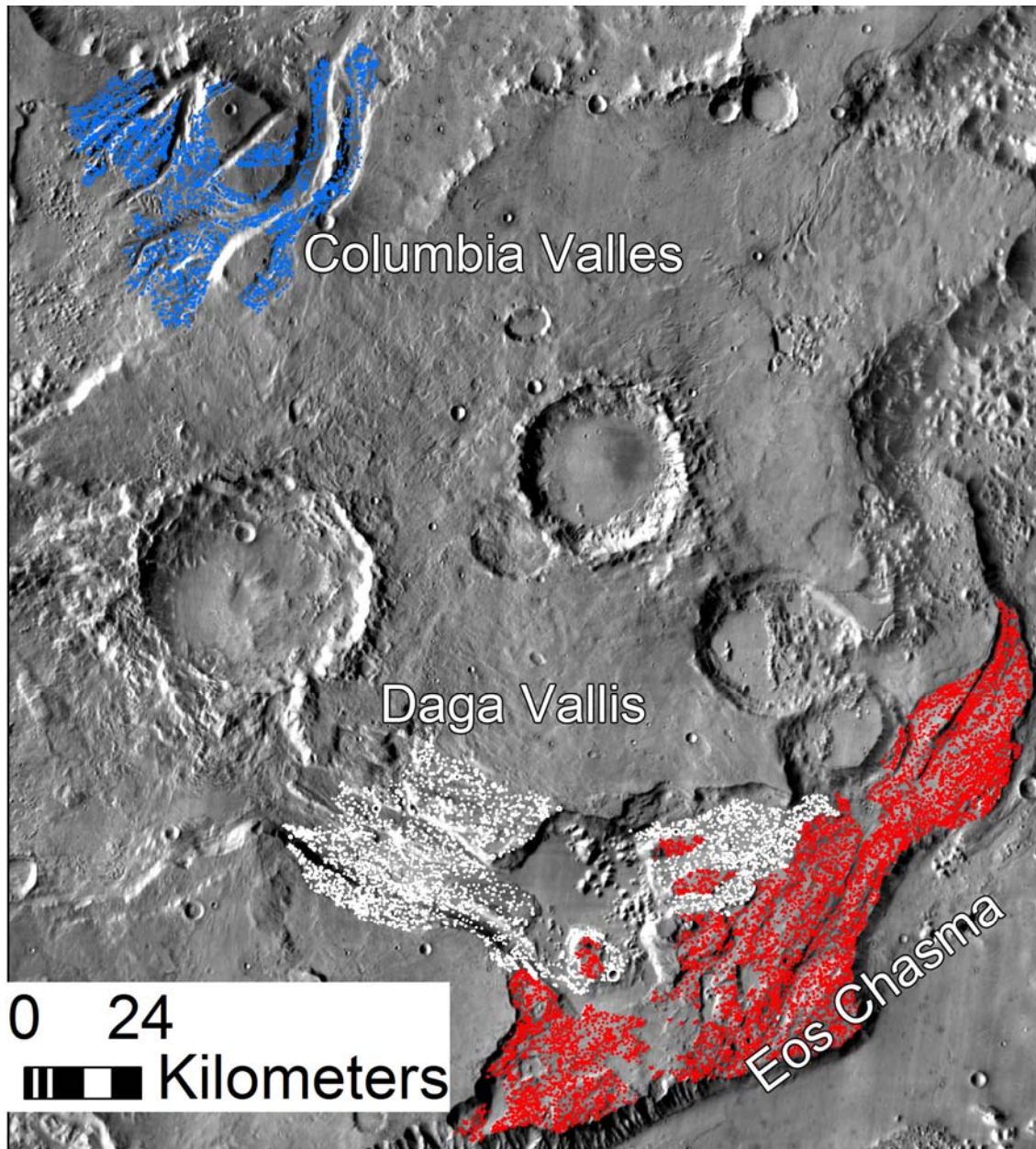


Figure DR7: THEMIS daytime IR mosaic of the three outflow channels targeted for our impact crater chronology analysis. The digitized impact craters ($D > 100$ m) are displayed.

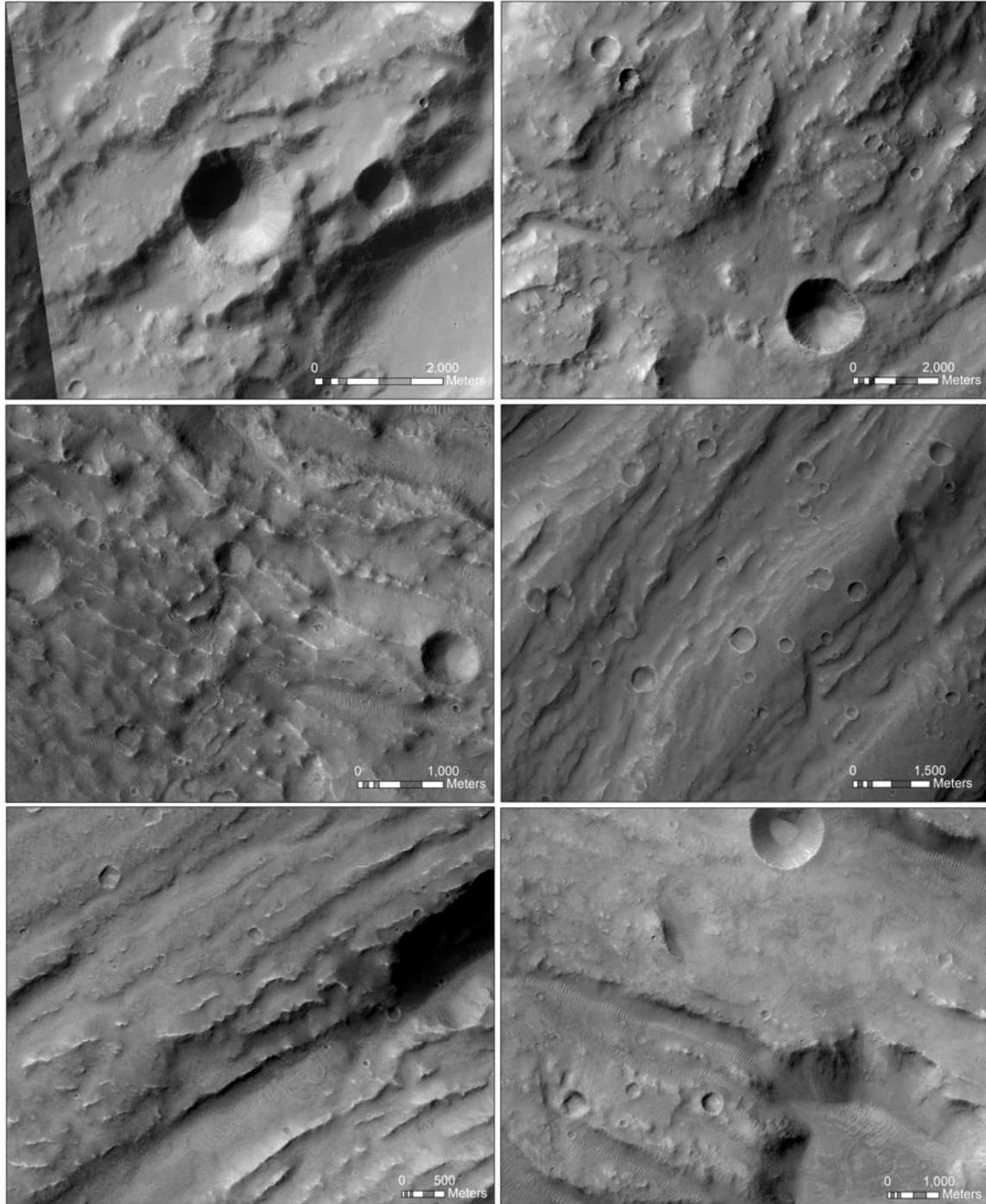


Figure DR8: Example impact structures on the floors of the outflow channels. Craters with $D > 200$ m are well-preserved and superimpose flood-related grooved terrain. This population thus formed after the flood erosion event. Few pre-flood impact craters were observed.

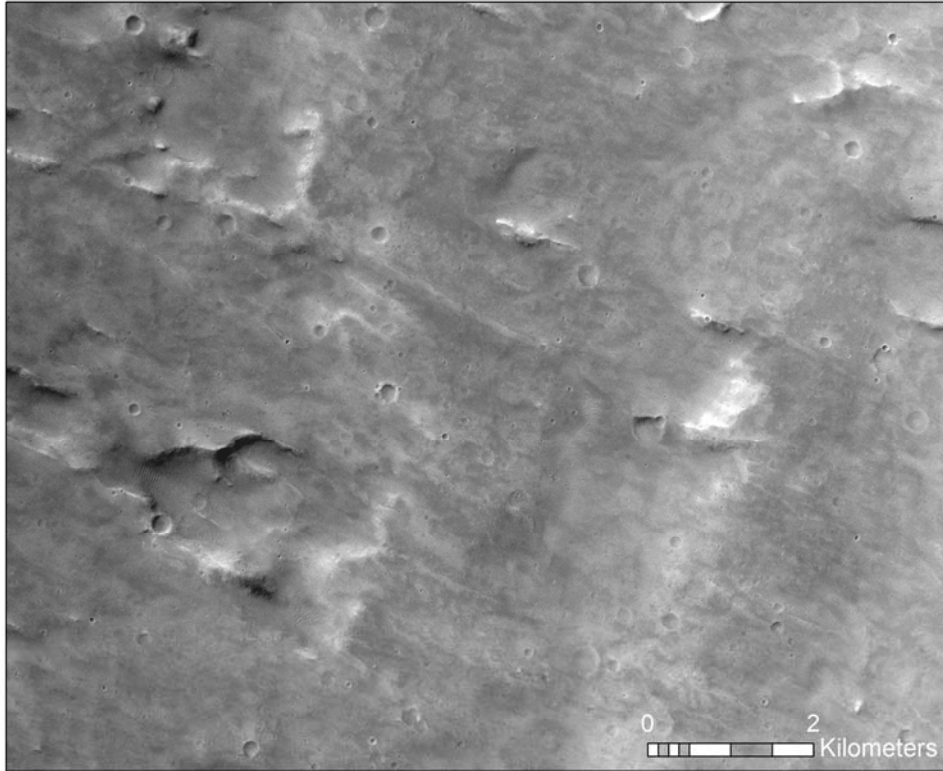


Figure DR9: Secondary chains associated with a 48-km-diameter crater located just northwest of Daga Vallis on Eos Mensa. The secondary chains within range of the outflow channels contain impact structures that are between 1 and 2 kilometers in diameter.

Table DR1: Complete list of CTX and HRSC images used in this study.

CTX images used in this study		
B01_009881_1648_XI_15S047W	P03_002128_1667_XI_13S047W	P13_006255_1717_XN_08S040W
B01_010026_1663_XN_13S045W	P04_002563_1648_XN_15S043W	P14_006479_1692_XN_10S036W
B01_010184_1722_XN_07S040W	P04_002642_1717_XI_08S041W	P14_006519_1688_XN_11S048W
B02_010580_1625_XN_17S050W	P05_002827_1651_XN_14S051W	P14_006624_1710_XN_09S035W
B03_010659_1667_XI_13S047W	P05_002866_1725_XI_07S037W	P14_006651_1644_XI_15S051W
B03_010804_1671_XI_12S046W	P05_002945_1712_XN_08S033W	P15_006743_1670_XN_13S044W
B03_010843_1744_XN_05S032W	P06_003301_1716_XN_08S032W	P15_006796_1649_XI_15S051W
B05_011503_1662_XN_13S050W	P06_003328_1656_XN_14S048W	P15_006822_1717_XN_08S041W
B05_011555_1672_XN_12S030W	P06_003367_1705_XN_09S033W	P15_006848_1723_XN_07S031W
B06_012017_1719_XN_08S043W	P06_003394_1652_XN_14S050W	P15_006888_1662_XN_13S043W
B08_012571_1672_XN_12S048W	P06_003407_1664_XN_13S045W	P15_006888_1662_XN_13S043W
B09_013151_1696_XN_10S043W	P06_003446_1721_XN_07S030W	P15_006914_1682_XN_11S033W
B09_013217_1717_XN_08S045W	P06_003473_1657_XN_14S047W	P15_006967_1681_XI_15S040W
B09_013283_1672_XN_12S046W	P06_003512_1713_XN_08S032W	P15_006980_1763_XN_03S036W
B10_013349_1671_XN_12S048W	P07_003578_1757_XI_04S035W	P15_007033_1695_XN_10S042W
B10_013481_1629_XN_17S052W	P07_003657_1724_XN_07S031W	P15_007099_1701_XN_09S044W
B10_013560_1663_XN_13S049W	P07_003684_1657_XN_14S047W	P16_007165_1662_XN_13S046W
B10_013718_1714_XN_08S044W	P07_003697_1644_XN_15S042W	P16_007178_1669_XN_13S041W
B11_013784_1715_XN_08S044W	P07_003789_1701_XN_09S034W	P16_007376_1622_XN_17S048W
B12_014179_1758_XI_04S030W	P07_003816_1652_XN_14S051W	P16_007389_1687_XI_11S043W
B16_015907_1719_XN_08S043W	P07_003895_1649_XN_15S048W	P16_007415_1766_XN_03S034W
B17_016144_1704_XN_09S034W	P08_003961_1652_XN_14S050W	P16_007442_1663_XI_13S050W
B17_016171_1680_XN_12S051W	P08_004013_1721_XN_07S030W	P17_007534_1644_XN_15S042W
B17_016210_1739_XN_06S036W	P08_004027_1645_XN_15S051W	P17_007639_1727_XN_07S030W
B17_016329_1671_XI_12S044W	P08_004040_1642_XN_15S046W	P17_007679_1695_XN_10S042W
B17_016421_1733_XN_06S037W	P08_004079_1713_XI_08S033W	P17_007732_1624_XN_17S048W
B17_016461_1684_XN_11S048W	P08_004264_1644_XN_15S042W	P17_007824_1666_XN_13S041W
B18_016566_1764_XN_03S036W	P08_004290_1713_XN_08S032W	P17_007837_1711_XN_08S037W
B18_016579_1760_XN_04S030W	P08_004317_1688_xi_11S049W	P18_007943_1637_XI_16S050W
B18_016606_1667_XN_13S047W	P09_004356_1704_XN_09S034W	P18_008061_1761_XN_03S033W
B18_016830_1716_XN_08S043W	P09_004396_1661_XI_13S046W	P18_008088_1652_XN_14S049W
B19_016856_1675_XN_12S032W	P09_004712_1729_XI_07S033W	P18_008180_1658_XN_14S042W
B19_017094_1688_XN_11S050W	P11_005174_1644_XN_15S046W	P19_008378_1672_XN_12S049W
B21_017740_1682_XN_11S047W	P11_005187_1706_XN_09S042W	P20_008681_1722_XN_07S044W
B21_017779_1761_XN_03S033W	P11_005200_1695_XN_10S036W	P20_008707_1757_XI_04S034W
B22_018096_1671_XN_12S046W	P11_005253_1710_XN_09S044W	P20_008747_1652_XN_14S045W
B22_018228_1622_XN_17S050W	P11_005332_1681_XN_11S040W	P20_008760_1672_XN_12S041W
B22_018241_1640_XN_16S044W	P11_005451_1663_XN_13S049W	P20_008773_1715_XN_08S036W
G01_018425_1714_XI_08S029W	P11_005464_1710_XI_09S044W	P20_008826_1712_XN_08S043W
G01_018650_1684_XI_11S051W	P11_005517_1620_XI_18S049W	P20_008918_1696_XN_10S035W
G02_019203_1746_XN_05S030W	P12_005543_1700_XI_10S041W	P20_009037_1718_XN_08S044W
G03_019362_1683_XN_11S050W	P12_005543_1700_XI_10S041W	P21_009103_1666_XN_13S047W
G03_019441_1653_XN_14S046W	P12_005662_1653_XN_14S049W	P21_009169_1667_XN_13S047W
G03_019546_1753_XN_04S034W	P12_005767_1691_XN_10S036W	P21_009380_1670_XN_13S047W
P01_001376_1676_XI_12S046W	P12_005807_1689_XI_11S048W	P22_009498_1734_XN_06S032W
P01_001389_1719_XN_08S041W	P12_005846_1717_XI_08S033W	P22_009538_1718_XN_08S044W
P02_001772_1670_XI_13S048W	P12_005899_1678_XN_12S040W	P22_009564_1725_XN_07S033W
P03_002049_1652_XN_14S050W	P12_005912_1703_XN_09S035W	P22_009617_1689_XN_11S039W
P03_002075_1720_XN_08S041W	P13_006123_1736_XN_06S036W	P22_009617_1689_XN_11S039W
P03_002101_1725_XN_07S031W	P13_006176_1666_XN_13S043W	P22_009670_1669_XN_13S047W

HRSC data used for the DTM mosaic			
h0533_0000	h2134_0000	h2123_0000	h2024_0001
h0394_0009	h2112_0000	h0018_0000	h0155_0001
h1863_0000	h2156_0000	h0478_0000	h2002_0001
h7201_0000	h2178_0000	h0456_0000	h2013_0001
h2222_0000	h0061_0008	h3158_0000	h1991_0000
h2211_0000	h0259_0000	h3147_0001	h1980_0000
h2145_0000	h3180_0000	h3125_0000	h2057_0000
h2101_0000	h2101_0000	h1969_0000	h3235_0001
h2123_0000	h2090_0000		

Table DR2: Crater statistics from the eastern Valles Marineris region.

Surface	Area (km ²)	Total Counts	N(0.1)	N(0.2)	N(0.5)	N(1)	N(2)	N(5)
Daga Vallis	2006	3868 +/- 62	1.93×10^6	5.21×10^5	1.59×10^4	2.49×10^3	4.98×10^2	NA
Eos Chasma	2841	7667 +/- 88	2.69×10^6	5.23×10^5	1.62×10^4	3.51×10^3	3.51×10^2	NA
Columbia Valles	1340	2920 +/- 54	2.18×10^6	5.36×10^5	1.64×10^4	2.24×10^3	7.46×10^2	NA
Capri Mensa (mantle)	3357	918 +/- 30	2.73×10^5	1.58×10^5	1.78×10^4	1.49×10^3	NA	NA
Eos Chaos (floor)	90183	38 +/- 6	NA	NA	NA	NA	4.21×10^2	1.21×10^2
Aurorae Chaos (floor)	119066	46 +/- 7	NA	NA	NA	NA	3.86×10^2	8.39×10^1

N(X) = (cumulative number of impact craters of X km diameter per 10^6 km²)